

Radiogalaxies in the Sloan Digital Sky Survey: spectral index-environment correlations

Carlos G. Bornancini^{1,2}, Ana Laura O’Mill^{1,2}, Sebastián Gurovich^{1,2} and Diego García Lambas^{1,2}

¹*Instituto de Astronomía Teórica y Experimental, IATE, Observatorio Astronómico, Universidad Nacional de Córdoba, Laprida 854, X5000BGR, Córdoba, Argentina.*

²*Consejo Nacional de Investigaciones Científicas y Técnicas (CONICET), Avenida Rivadavia 1917, C1033AAJ, Buenos Aires, Argentina.*

30 October 2018

ABSTRACT

We analyze optical and radio properties of radiogalaxies detected in the Sloan Digital Sky Survey (SDSS). The sample of radio sources are selected from the catalogue of Kimball & Ivezić (2008) with flux densities at 325, 1400 and 4850 MHz, using WENSS, NVSS and GB6 radio surveys and from flux measurements at 74 MHz taken from VLA Low-frequency Sky Survey (Cohen et al. 2006). We study radiogalaxy spectral properties using radio colour-colour diagrams and find that our sample follows a single power law from 74 to 4850 MHz. The spectral index vs. spectroscopic redshift relation ($\alpha - z$) is not significant for our sample of radio sources. We analyze a subsample of radio sources associated with clusters of galaxies identified from the maxBCG catalogue and find that about 40% of radio sources with ultra steep spectra (USS, $\alpha < -1$, where $S_\nu \propto \nu^\alpha$) are associated with galaxy clusters or groups of galaxies. We construct a Hubble diagram of USS radio sources in the optical r band up to $z \sim 0.8$ and compare our results with those for normal galaxies selected from different optical surveys and find that USS radio sources are around as luminous as the central galaxies in the maxBCG cluster sample and typically more than 4 magnitudes brighter than normal galaxies at $z \sim 0.3$.

We study correlations between spectral index, richness and luminosity of clusters associated with radio sources. We find that USS at low redshift are rare, most of them reside in regions of unusually high ambient density, such of those found in rich cluster of galaxies. Our results also suggest that clusters of galaxies associated with steeper than the average spectra have higher richness counts and are populated by luminous galaxies in comparison with those environments associated to radio sources with flatter than the average spectra. A plausible explanation for our results is that radio emission is more pressure confined in higher gas density environments such as those found in rich clusters of galaxies and as a consequence radio lobes in rich galaxy clusters will expand adiabatically and lose energy via synchrotron and inverse Compton losses, resulting in a steeper radio spectra.

Key words: surveys – radio continuum: general – radio continuum: galaxies – galaxies: high-redshift

1 INTRODUCTION

Radio sources are frequently associated with massive systems at low and high redshifts. In the Local Universe these objects are usually identified with evolved red ellipticals and with luminous cD galaxies located at the centres of clusters of galaxies (West 1994). Radio sources at high redshifts ($z \sim 4$) are identified with massive forming systems, i.e galaxies with diffuse UV morphologies and consistent

with small substructures around a dominant bright galaxy (Miley et al. 2006).

Several works show that some distant radio sources are embedded in highly spatially extended ionized gas nebulae of 100-200 kpc (Venemans et al. 2002; Villar-Martín et al. 2007). These gas structures are observed in massive ellipticals or cD galaxies at the center of nearby clusters of galaxies. This evidence suggests that distant radio sources represent the progenitors of the most massive galaxies observed

in the Local Universe and therefore important for the study of structure formation, such as clusters or groups of galaxies.

A high fraction of radio sources associated with clusters of galaxies have steep radio spectra as measured by the slope between two fixed ranges of frequencies, i.e the spectral index α (USS, $\alpha < -1$, where $S_\nu \propto \nu^\alpha$, Roettgering et al. (1997); Chambers et al. (1996); Jarvis et al. (2001)). Such a correlations between spectral index and redshift ($\alpha - z$ relation), has been used with success to search for distant galaxies (De Breuck et al. 2000; Jarvis et al. 2004; Cruz et al. 2006; Broderick et al. 2007).

There are at least three main explanations given in the literature for this phenomenon: The first is a radio k-correction. The spectral energy distribution (SED) of radio sources is usually concave, i.e the spectral index increases with frequency. The observed spectral index determined from two fixed observed frequencies will therefore sample a steeper part of the radio spectrum for sources at higher redshifts. The second is related with the interaction between photons of the cosmic microwave background radiation (CMB) and the relativistic electron population observed in the plasma gas of radio sources. The energy density of the CMB increases as $(1+z)^4$ and hence Inverse Compton scattering (IC) of the CMB becomes increasingly important for sources at high redshifts (Krolik & Chen 1991). The third is related to an intrinsic correlation between radio luminosity and *rest-frame* spectral index (Blundell & Rawlings 1999a; Chambers et al. 1990) that due to a Malmquist like bias in flux density limited surveys translates into a correlation between spectral index and redshift. An alternative explanation is related with an ambient density effect. The presence of USS radio sources residing closest to cluster centres may be due to a manifestation of pressure-confined radio lobes which slow adiabatic expansion of the plasma. Radio lobes will be pressure-confined and lose energy primarily via synchrotron and IC losses (Klamer et al. 2006).

Studies of radio sources at low and moderate redshifts ($z < 0.5$) show different environments.

Hill & Lilly (1991) find that only 50% of powerful radio sources at $z \sim 0.5$ are located in rich galaxy clusters, even though similar sources avoid such environments at low redshifts. However, Geach et al. (2007) analyzed radio sources in the Subaru/XMM-Newton Deep Field and found that low-power radio galaxies at $z \sim 0.5$ reside in moderately rich groups - intermediate environments between poor groups and rich clusters.

Prestage & Peacock (1988) investigate the local galaxy density around powerful radio sources using the angular cross-correlation technique and find that compact radio sources appear to lie in regions of low galaxy density. Moreover, that complex Fanaroff-Riley class I sources are typically found in regions of significantly enhanced galaxy density.

Allington-Smith et al. (1993) study the evolution of galaxies in radio-selected groups at $z < 0.5$ with the same range of radio power and find that strong radio galaxies are located in a wide range of environments but not as wide as for groups in general. At low redshifts ($z < 0.1$) radio-selected groups have the same richness and blue fraction as do optically-selected groups. At high redshifts ($z \sim 0.4$) all groups have the same proportion of blue galaxies.

Studying the prevalence of radio loud AGN activity in

nearby groups and galaxy clusters, selected from the SDSS catalog, Best et al. (2007) find that brightest group and cluster galaxies are more likely to host a radio loud AGN than other galaxies of the same stellar mass.

In this work we analyze optical and radio properties of radio sources with steep radio spectra, and we determine the main characteristics of clusters of galaxies associated with radio sources.

The structure of this paper is organized as follows: Section 2 describes the optical and radio samples analyzed. We analyze radio spectral properties of our sample in Section 3. Section 4 compares the optical and the radio luminosities of sources associated with steep spectrum and central galaxy clusters. In section 5, we study the Hubble diagram in the optical r band for USS sources. We study in Section 6 spectral index and richness properties of galaxies associated with clusters of galaxies and finally, in Section 7, we discuss our main results.

Throughout this work we assume a standard Λ CDM model Universe with cosmological parameters, $\Omega_M=0.3$, $\Omega_\Lambda=0.7$ and a Hubble constant of $H_0=100 \text{ h km s}^{-1} \text{ Mpc}^{-1}$.

2 RADIO AND OPTICAL GALAXY SAMPLES

The sample of radio sources was selected from the catalogue of Kimball & Ivezić (2008). This catalogue presents information in radio and optical bands taken from several surveys, including Faint Images of the Radio Sky survey (FIRST, 1400 MHz), NRAO VLA Sky Survey (NVSS, 1400 MHz), Westerbork Northern Sky Survey (WENSS, 325 MHz), Green Bank survey (GB6, 4850 MHz), and the Sloan Digital Sky Survey (SDSS) optical survey. The flux density limits for each radio catalogue are 1, 2.5, 18 and 18 mJy for the FIRST, NVSS, GB and WENSS surveys, respectively.

The SDSS catalogue contains flux densities of detected objects measured nearly simultaneously in u, g, r, i, and z optical bands (Fukugita et al. 1996) with a limiting magnitude of $r < 22.2$ in an area of $\sim 10^4$ square degrees in the North Galactic cap and a small region of 225 square degrees in the South Galactic cap.

The sample of optical galaxies in the fields of radio sources were selected using the Catalog Archive Server Jobs System (CASJOBS) interface of SDSS, which allows one to obtain catalogues with parameters from the SDSS survey (DR6).¹

The matching radius to correlate the radio (FIRST) and optical (SDSS) surveys was $2''$. We chose this matching radius in order to avoid contamination by line of sight matches of physical unrelated objects, since Kimball & Ivezić (2008) previously found an efficiency (fraction of matches which are physically real) of 95% and completeness (fraction of real matches that were found) of 98% with this matching radius. In this work we used the following catalogue subsets: Sample D (detected by FIRST, NVSS and WENSS survey, with 63,660 sources), sample E (detected by FIRST, NVSS, WENSS, GB6 and the SDSS survey, 4732 sources) and sample G (detected by FIRST, NVSS, WENSS and the SDSS spectroscopic survey, 2885 sources). For all these samples

¹ <http://casjobs.sdss.org/CasJobs/>

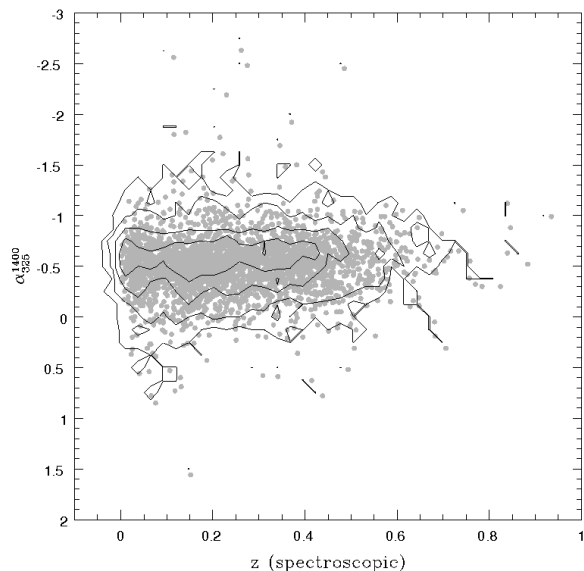


Figure 1. Spectral index, α_{325}^{1400} , vs. spectroscopic redshift from the SDSS catalogue for radio sources detected in FIRST (1.4 GHz), NVSS (1.4 GHz), WENSS (325 MHz) and the SDSS spectroscopic catalogue with a matching radius of $2''$. The contours represent the 50, 70, 80 and 90% of total objects.

Kimball & Ivezić (2008) estimated matching efficiencies of $> 80\%$ and completeness limits of $> 90\%$, using an appropriate matching radius.

A more detailed description of the radio sample and the criteria used to merge catalogues can be found in Kimball & Ivezić (2008).

Our sample of tracer galaxies for this work are drawn from the catalogue of galaxies with photometric redshifts of the DR6 catalogue (Oyaizu et al. 2008). These photometric redshifts were calculated using a Artificial Neural Network technique and the Nearest Neighbor Error (NNE) method to estimate photo- z errors for 77 million objects classified as galaxies in DR6 with $r < 22$. In order to study and analyze the properties of clusters of galaxies associated with radio sources, we correlate the radio sources detected from the FIRST, NVSS and WENSS catalogues with clusters of galaxies selected from the maxBCG survey (Koester et al. 2007a) using a matching radius of $10''$. The maxBCG catalogue includes 13,823 clusters selected from the SDSS photometric data, using two well-known features of rich clusters of galaxies: the red-sequence observed as a ridge line in the colour-magnitude diagram (the E/S0 ridgeline) and the presence of a bright dominant central galaxy (BCG). The catalogue includes the position, cluster photometric redshifts, BCG spectroscopic redshifts, $r e i$ total galaxy luminosities and luminosities of the central galaxies, the cluster richness, N_{gal} calculated as the number of galaxies projected within $1 h^{-1}$ Mpc, brighter than $0.4L_*$ and with colours matching the E/S0 ridgeline, the cluster richness within R_{200} from the cluster center, defined as the mean density of 200 times the mean density of the Universe (see for instance Koester et al. (2007b)).

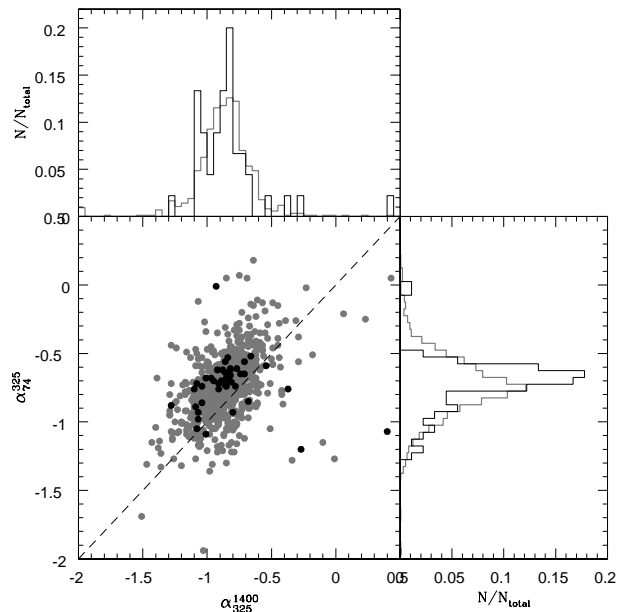


Figure 2. Radio Colour-colour diagram distributions for sources in the VLSS (74 MHz), WENSS (325 MHz) and NVSS (1.4 GHz) samples (grey circles). Filled circles represent measurements obtained for radio sources associated with maxBCG clusters. The dashed line indicates the relation for radio sources whose spectra follow a single power law from 74 to 1400 MHz. Histograms represent the corresponding distribution of spectral index.

3 RADIO PROPERTIES

3.1 $\alpha - z$ relation

In Figure 1 we plot spectral index α_{325}^{1400} vs. spectroscopic redshift for radio sources identified in the SDSS catalogue. The data were obtained from the catalogue subset G taken from Kimball & Ivezić (2008). The contours represent the 50, 70, 80 and 90% of total objects. We do not find a tendency of α with redshift, showing that the most distant ($z > 0.5$) radio galaxies in our sample do not show steep spectra due to a k-correction effect applied to a concave radio SED.

3.2 Analysis of the SED in radio frequencies

In order to study radiogalaxy properties we analyze radio colour-colour diagrams. In Figure 2 we show the radio two-colour diagram which compares the spectral index at 74-352 MHz and 352-1400 MHz. We use the CATS database of the Special Astronomy Observatory (Verkhodanov et al. 1997) in order to obtain flux measurements at 74 MHz taken from the VLA Low-frequency Sky Survey (VLSS) (Cohen et al. 2006), using a matching radius of $60''$ for the FIRST and NVSS samples. Grey circles represent sources detected in the FIRST, NVSS and WENSS catalogues (listed as Sample D in Kimball & Ivezić (2008)). Filled circles represent data for radio sources associated with clusters of galaxies identified in the maxBCG catalogue. The dashed line indicates the relation for radio sources whose spectra follow a single power law from 74 to 1400 MHz. Again, we do not

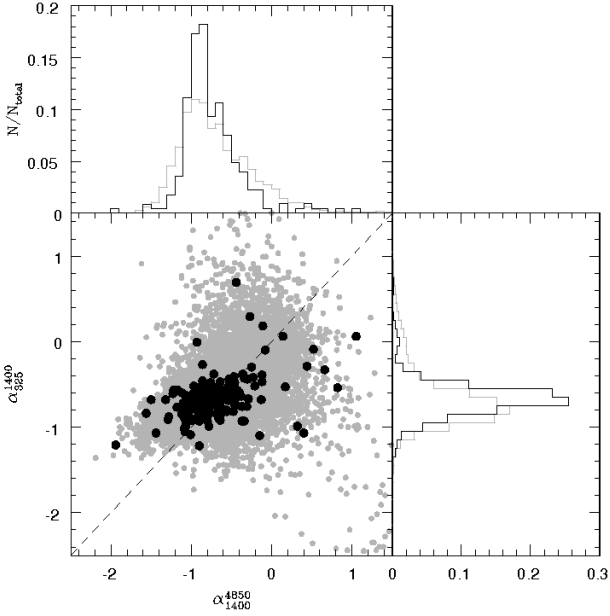


Figure 3. Radio Colour-colour diagram distributions for sources in the WENSS (325 MHz), NVSS (1.4 GHz) and GB6 (4.85 GHz) samples (grey circles). Filled circles represent measurements obtained for radio sources associated with maxBCG clusters. The dashed lines correspond to a single power law spectra from 325 to 4850 MHz. Histograms represent the corresponding distribution of spectral index.

find a clear tendency that most of radio sources show some flattening towards low frequencies. In Figure 3 we show a similar analysis for radio sources with radio emission in 325, 1400 and 4850 MHz, listed as Sample E in Kimball & Ivezić (2008) (grey circles). Filled circles represent data obtained for radio sources identified with clusters of galaxies detected in the maxBCG catalogue. The equal number of points on either side of this line indicate no significant spectral curvature.

4 OPTICAL AND RADIO LUMINOSITIES

In order to study radio source luminosity properties at optical and radio frequencies as well as other possible correlations, we calculated the *rest-frame* radio luminosity at 1.4 GHz:

$$L_{1.4} = 4\pi D_L^2(z) S_{1.4} (1+z)^{-(1+\alpha)}, \quad (1)$$

where $D_L(z)$ is the luminosity distance in the adopted Λ -CDM cosmology, $S_{1.4}$ is the observed flux density at 1.4 GHz and $(1+z)^{-(1+\alpha)}$ is the standard k-correction term used in radio frequencies.

In Figure 4 we show the luminosity distribution of radio sources associated with maxBCG clusters (shaded histogram) and USS ($\alpha_{325}^{1400} < -1$) radio sources with spectroscopic redshifts (solid line histogram). The dashed line histogram shows the distribution for radio sources without a maxBCG cluster association. We note the good agreement between these three distributions, indicating that most of

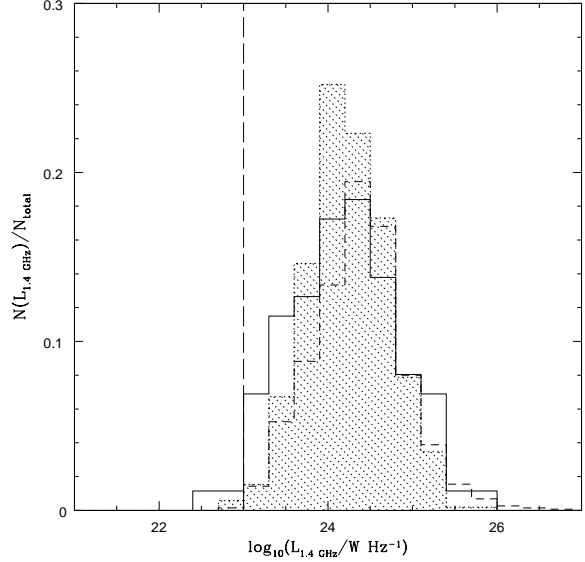


Figure 4. Radio luminosity distribution in 1.4 GHz. Shaded histogram represents the luminosity distribution for maxBCG clusters detected in the FIRST, NVSS and WENSS survey. Dashed line histogram shows the distribution for radio sources without a maxBCG cluster association. Solid line histogram represents the distribution for USS sources. Dashed line shows the criterion for radio-loud radio sources ($L_{1.4\text{GHz}} > 10^{23} \text{ W Hz}^{-1}$)

the radio sources associated with central clusters of galaxies and USS sources are radio-loud ($L_{1.4\text{GHz}} > 10^{23} \text{ W Hz}^{-1}$). Several works show a correlation between spectral index and radio luminosity (or radio power) (e.g., Blundell et al. 1999b; Gopal-Krishna 1988; Laing & Peacock 1980). As can be seen, we do not find any trend in radio luminosity and spectral index for these subsamples of radio sources. It should be noted that the results shown in this figure are not likely to be biased by possible luminosity selection effects in steep spectral index sources.

To obtain absolute magnitudes in the r band we use the de-reddened model magnitudes and k-correct using the V4.1 public code of Blanton & Roweis (2007). Figure 5 shows the distribution of absolute r band magnitude for USS radio sources (solid line histogram) and for central cluster objects in the maxBCG catalogue (shaded line histogram). The dashed line histogram shows the distribution obtained for radio sources associated with maxBCG clusters. As can be seen there is only a small difference between the two samples, where USS radio sources are marginally brighter than the central galaxies associated with maxBCG clusters.

5 HUBBLE DIAGRAM IN THE R BAND

In the last three decades the Hubble diagram in the K -band ($K-z$ diagram) has been used to detect and study distant radio galaxies. One of the first works using the Hubble diagram was published by Lilly & Longair (1984) using a sample of radio sources detected in the 3CR catalogue. The first radiogalaxy identified at $z > 3$ in fact was selected at radio frequencies as a faint source in the K -band (Lilly

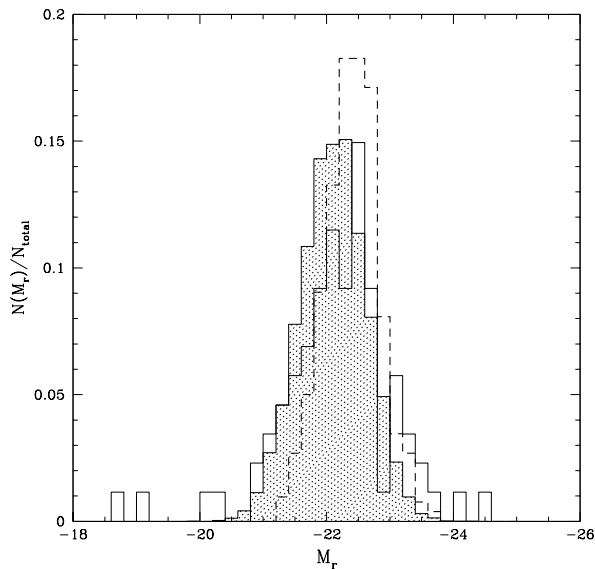


Figure 5. Absolute magnitude distribution in r band. Shaded histogram represents the distribution for central galaxies in the maxBCG cluster catalogue. Solid and dashed line histograms show the corresponding distribution for USS sources and for radio sources associated with clusters of galaxies identified in the maxBCG catalogue, respectively.

1988). This technique was used in combination with spectral index cuts and rejecting radio sources with large angular sizes ($< 30''$) (De Breuck et al. 2000, 2002; Cohen et al. 2004; Cruz et al. 2006).

In this work we perform a similar analysis in the optical r band. Figure 6 shows the Hubble diagram using the r band (petrosian magnitudes) vs. spectroscopic redshift. Filled circles represent measurements obtained for USS objects, big circles represent radio sources associated to maxBCG clusters. Light grey circles correspond to galaxies detected in the SDSS catalogue within the NOAO Deep Wide-Field Survey area, with photometric redshifts taken from (Oyaizu et al. 2008). Dark grey points represent measurements of galaxies detected in the VIMOS VLT deep survey (VVDS-DEEP) (Le Fevre et al. 2005), with spectroscopic redshift and magnitudes converted to the SDSS system². Crosses represent spectroscopic measurements for galaxies identified in the Hubble Deep Field North region obtained in the ACS-GOODS survey (Cowie et al. 2004). The solid line represents the best fit obtained for the USS source sample, $r = (4.46 \pm 0.21) \times \log_{10}(z) + (20.28 \pm 0.16)$. As can be seen, USS radio sources are typically more than 4 magnitudes brighter than normal galaxies at $z \sim 0.3$. In Figure 7 we plot a similar Hubble diagram for radio sources with spectroscopic redshift quoted in sample G from Kimball & Ivezić (2008) (grey points). Open red triangles represent measurements obtained for maxBCG clusters with radio emission and USS radio sources are displayed with open squares. The solid line represents the best fit obtained for the USS source sample. USS radio sources follow a similar distribution in

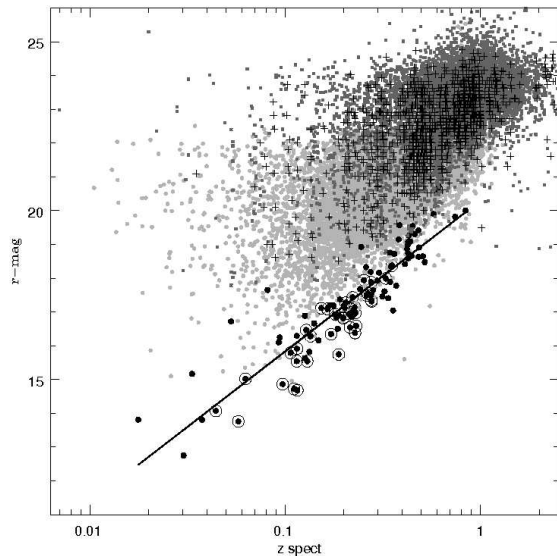


Figure 6. Hubble diagram in the r band vs. spectroscopic redshift taken from the SDSS catalogue. Filled circles represent measurements obtained for USS objects. USS radio sources identified with maxBCG clusters are displayed as big circles. Light grey circles correspond to galaxies detected in the SDSS catalogue in the NOAO Deep Wide-Field Survey area with photometric redshifts taken from (Oyaizu et al. 2008). Dark grey points represent measurements of galaxies detected in the VIMOS VLT deep survey (VVDS-DEEP) (Le Fevre et al. 2005) with spectroscopic redshift and magnitudes converted to the SDSS system. Crosses represent spectroscopic measurements for galaxies identified in the Hubble Deep Field North region obtained in the ACS-GOODS survey (Cowie et al. 2004). The solid line represents the best fit line obtained for the USS source sample.

comparison with that obtained in the maxBCG cluster sample in the redshift range $0.1 < z < 0.3$. We find that USS sources are typically as luminous as the central galaxies in the maxBCG cluster sample. In the next Section, we analyze the nature of USS sources detected at low redshifts ($z < 0.1$).

6 ULTRA STEEP SPECTRUM SOURCES

In order to study the nature of radio sources with ultra steep spectra at low redshifts, we select a set of galaxies detected by NVSS, FIRST, WENSS, and SDSS with spectroscopic redshifts (catalogue subset G in Kimball & Ivezić (2008)). We use the NED database³ to search for known objects present in the literature and find that 40% of USS sources are associated with clusters or groups of galaxies identified in the maxBCG (Koester et al. 2007a), Abell (Abell et al. 1989), Zwicky (Zwicky & Kowal 1968) catalogues and Northern Sky optical Cluster Survey (NSCS, Lopes et al. (2004)) catalogues. Table 1 lists the sample of USS sources identified with galaxies with optical spectra in the SDSS catalogue. The columns are the following: ID taken

² <http://www.sdss.org/dr4/algorithms/sdssUBVRITransform.html>

³ <http://nedwww.ipac.caltech.edu/> the NASA-IPAC Extragalactic Database.

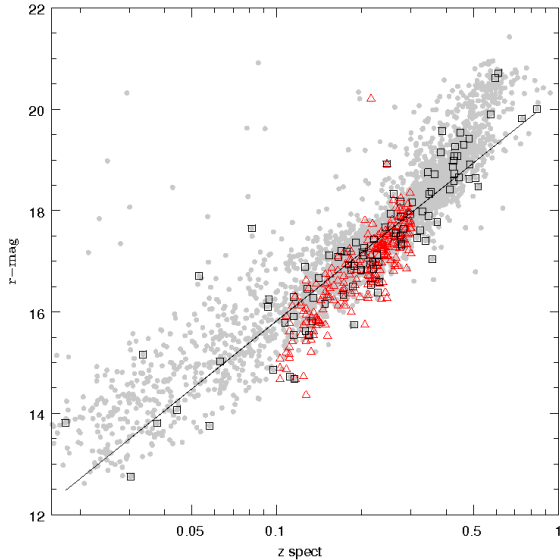


Figure 7. Hubble diagram in the r band vs. redshift. Radio sources with spectroscopic redshift measurements (grey points). Open red triangles represent measurements obtained for maxBCG clusters with radio emission. USS radio sources are displayed with open squares.

from Kimball & Ivezić (2008), position, spectroscopic redshift, spectral index obtained between 352MHz and 1.4 GHz, 1.4 GHz radio luminosity, r band absolute magnitude, and ID taken from literature. In Figure 14 we show a sample of colour images of radio sources with $\alpha_{325}^{1400} < -1$. At low redshift ($z < 0.1$) we find that most USS sources are associated with nearby bright spiral galaxies or interacting systems, with a possible AGN. This may be due to the low limiting flux density used ($S_{1400} = 2.5$ mJy, from the NVSS survey) since we note that De Breuck et al. (2000) found that they can select against low redshift spiral galaxies among USS sources by selecting sources with $S_{1400} > 10$ mJy.

Some radio sources that are associated to bright red galaxies are located in similar density environments as those found in clusters or groups of galaxies, but do not have a cluster association in the literature. In the next Section we analyze the galaxy density associated with these systems.

7 SPECTRAL INDEX AND RICHNESS

In order to study the nature of radio sources associated to clusters of galaxies we analyze possible correlations between spectral index, the richness associated with each cluster and the luminosity properties of galaxies in these environments. The spectral index (α_{325}^{1400}) distribution for radio sources detected in FIRST, NVSS and WENSS catalogues (listed as Sample D) not associated with a maxBCG cluster can be seen in Figure 8 (shaded histogram). The solid line histogram represents the corresponding spectral index distribution for radio sources associated with maxBCG clusters. The mean value distribution for clusters is $\bar{\alpha}_{325}^{1400} = -0.65$. We find a tendency that most radio sources associated with maxBCG clusters have steep radio spectra in comparison

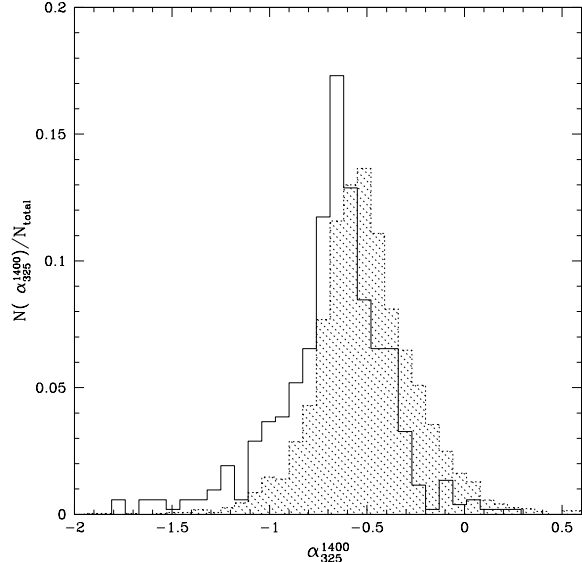


Figure 8. Spectral index α_{325}^{1400} distribution for radio sources without a maxBCG match (shaded histogram) and with a maxBCG cluster match (solid lines).

with field radio sources at similar redshifts. This result is in agreement with Baldwin & Scott (1973) and Slingo (1974), who also find that nearby radio sources with steep spectra reside in rich clusters of galaxies.

In Figure 9 we plot the absolute r band magnitude of central maxBCG cluster galaxies vs. richness (N_{gal}) for each cluster associated to radio sources with steeper than average, $\alpha_{325}^{1400} < -0.65$ (filled grey circles) and with flatter than average spectra, $\alpha_{325}^{1400} > -0.65$ (open circles), respectively. The contours represent the 90% of total objects (grey line) for steep sources, solid line for flat sources and dashed lines for maxBCG clusters without radio emission. We find that clusters of galaxies associated with steep spectrum sources have brighter central galaxies and have a high galaxy richness in comparison with clusters associated with flatter than the average radio sources.

In order to provide a suitable calibration to help the reader judge how Abell richness counts relate to the N_{gal} values, we show in Figure 10 this correlation using the revised northern Abell Catalog (Abell et al. 1989). As it can be appreciated in this figure, although with a large scatter, there is a positive correlation between these richness estimates. Abell richness class $R = 0$ clusters have commonly $N_{\text{gal}} \sim 20$, while objects with richness class 2 correspond to $N_{\text{gal}} > 30$.

In Figure 11 we present the distribution of richness (N_{gal}) for clusters of galaxies taken from the maxBCG catalogue calculated from the red-sequence of the colour-magnitude diagram. We plot in solid line the richness distribution of radio sources with $\alpha_{325}^{1400} < -0.65$. The shaded histogram represents the distribution for radio sources with $\alpha_{325}^{1400} > -0.65$ and the dashed line histogram the richness distribution for maxBCG clusters without radio emission. We find a tendency that radio sources with steeper than the average spectra are found preferentially in higher galaxy

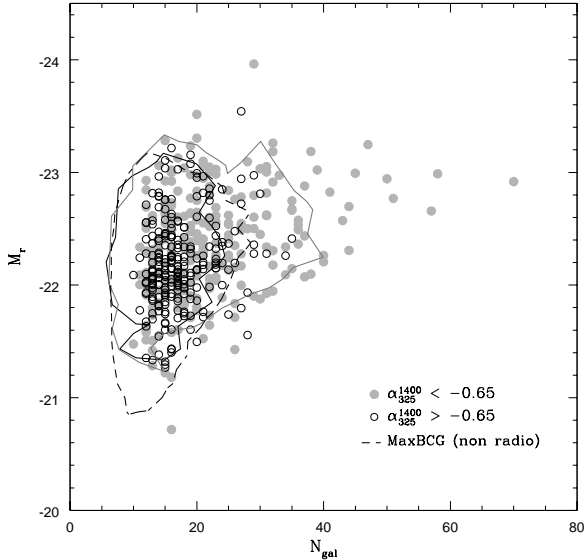


Figure 9. Absolute magnitude in the r band of central maxBCG cluster galaxies as a function of galaxy richness (N_{gal}). Grey circles represent measurements for clusters associated with radio sources with $\alpha_{325}^{1400} < -0.65$ and black circles represent clusters identified with sources with $\alpha_{325}^{1400} > -0.65$. The contours represent the 90% of total objects (grey line for steep sources, solid line for flat sources and in dashed lines for maxBCG clusters without radio emission).

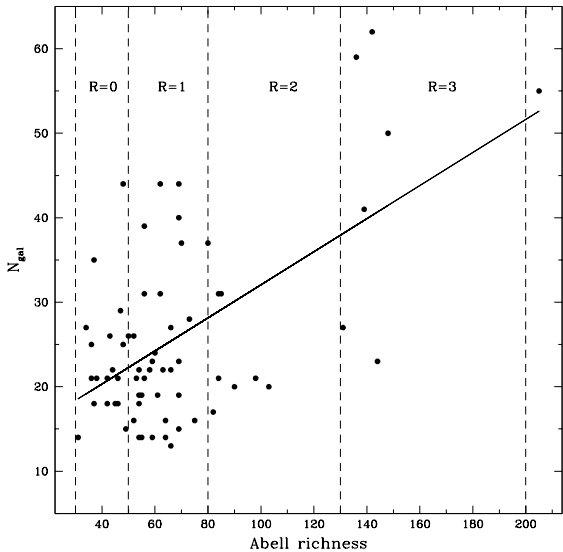


Figure 10. Abell richness vs. maxBCG richness N_{gal} from (Koester et al. 2007a). Dashed lines show the corresponding Abell richness group. Solid line represents the best fit obtained for these parameters.

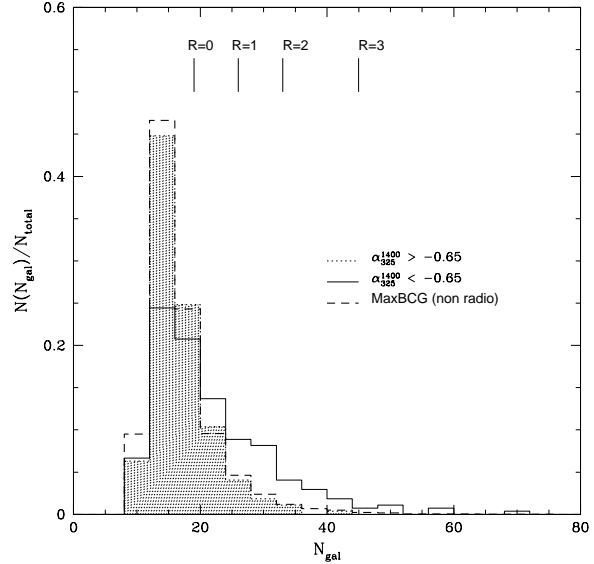


Figure 11. Galaxy richness distribution for maxBCG clusters in the WENSS–NVSS catalogues. The solid line histogram represents the richness associated to radio sources with $\alpha_{325}^{1400} < -0.65$ and the shaded histogram corresponds to sources with $\alpha_{325}^{1400} > -0.65$. The dashed line histogram shows the distribution for maxBCG clusters without radio emission. The corresponding Abell richness class are marked at the top of the figure.

richness environments than are radio sources with flatter than the average spectra.

For reference, we have also indicated in this figure the mean values of N_{gal} corresponding Abell richness class 0, 1, 2 and 3.

In order to compare the N_{gal} richness to other cluster parameters, we note the relation N_{gal} and R_{200} ($R_{200} \sim N_{gal}^{0.6}$) (See figure 7, Hansen et al. 2005)

In Figure 12 we plot the total r band luminosity of galaxies for clusters of galaxies associated with radio sources with $\alpha_{325}^{1400} < -0.65$ (solid line histogram) and those with ($\alpha_{325}^{1400} > -0.65$) as a shaded histogram. The dashed line histogram represents the distribution obtained for maxBCG clusters without radio emission. We find that radio sources with steeper than average spectra in central clusters of galaxies are populated by luminous galaxies in comparison with radio sources with flatter than average spectra. In contrast clusters of galaxies without radio emission have a lower distribution of total galaxy luminosity.

In a similar way, we analyze the density of galaxies associated with different types of radio sources. In Figure 13 left panel, we show the projected galaxy density using the 5th nearest neighbour in the plane of sky (Σ_5 , O’Mill et al. (2008)) as a function of spectral index for maxBCG clusters with $0.2 < z < 0.3$. The dashed line shows the USS criterion. Galaxies were selected with a range of radial velocity difference (ΔV), adopting a fixed $\Delta V = 1000 \text{ km s}^{-1}$ (for $z < 0.3$) and a varying $\Delta V = 1000\text{--}3000 \text{ km s}^{-1}$.

In Figure 13 right panel, we plot the projected density of galaxies within $1 h^{-1} \text{ Mpc}$ and with photometric redshifts in the range $\Delta z = 0.01$ from the central cluster galaxies (N1) as a function of the spectral index for clusters in the redshift

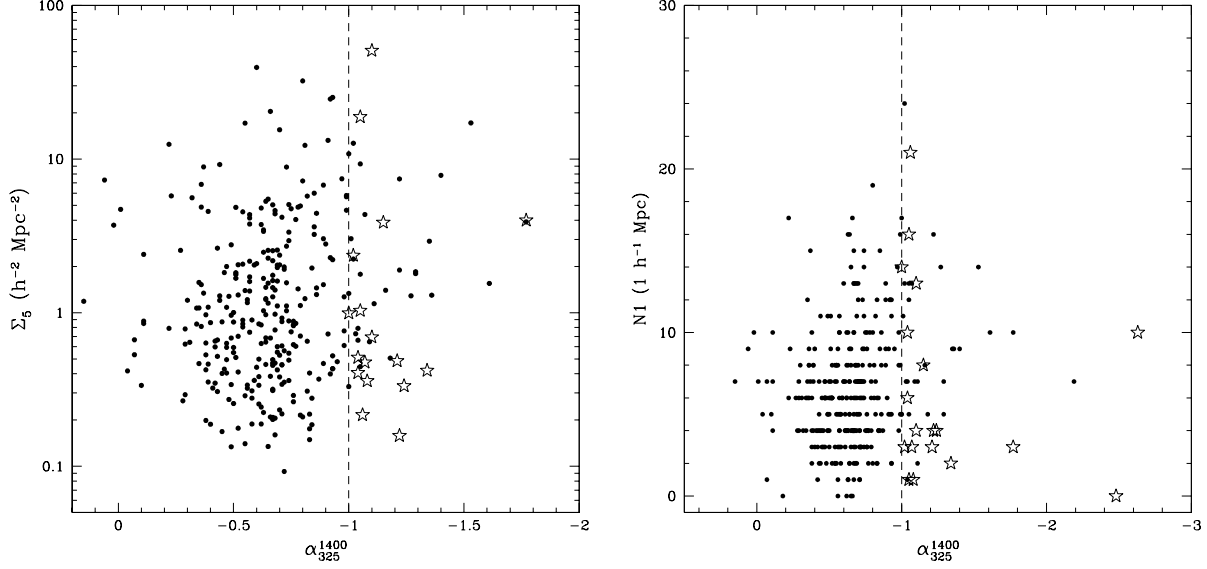


Figure 13. Left panel: Logarithm of the 5th nearest neighbour local galaxy density estimator (Σ_5) as a function of the spectral index for maxBCG clusters. Dashed vertical line show the selection criterion for USS sources. Right panel: Projected density of galaxies within $< 1 h^{-1} \text{ Mpc}$ vs. spectral index α_{325}^{1400} for cluster of galaxies in the maxBCG catalogue (filled circles). The projected density was calculated as a number of galaxies with photometric redshifts in the range $\Delta z=0.01$ from the BCG in the cluster in the redshift range $0.2 < z < 0.3$. Stars represent values obtained for the USS without a maxBCG cluster association.

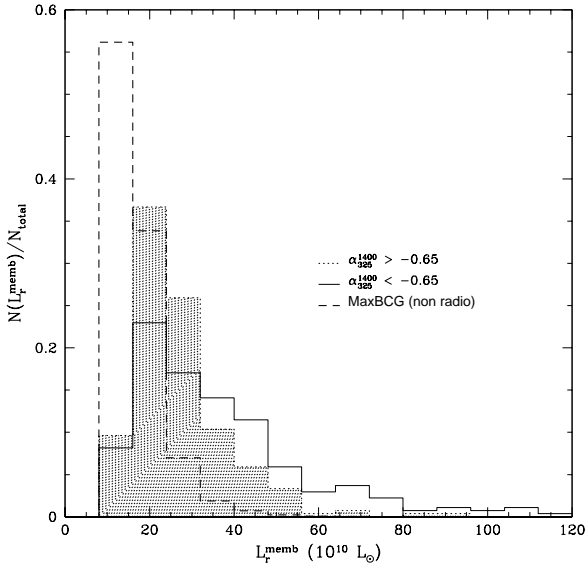


Figure 12. Total luminosity distribution for galaxies associated with maxBCG clusters detected in the WENSS–NVSS catalogues. Solid line histogram corresponds to radio sources with $\alpha_{325}^{1400} < -0.65$ and the shaded histogram represents the corresponding distribution for sources with $\alpha_{325}^{1400} > -0.65$. The dashed line histogram shows the distribution obtained for maxBCG clusters without radio emission.

range $0.2 < z < 0.3$ (filled circles). Stars represent the same values obtained for USS radio sources without a know cluster association, from the literature. As can be seen in both plots, we found that these USS sources inhabit environments with

galaxy densities similar to those clusters selected from the maxBCG catalogue.

8 CONCLUSIONS

We study optical and radio properties of radiogalaxies detected in the Sloan Digital Sky Survey (SDSS) with flux densities of 74, 325, 1400 and 4850 MHz, using the VLSS, WENSS, NVSS and GB6 radio catalogues. We search for a possible empirical correlation between the spectral index and redshift, however we find no significant trend. We analyze the functional form of the SED using colour-colour diagrams at radio frequencies. We do not find a clear tendency of radio sources to show flattening towards low frequencies, as expected assuming concave curvature in the radio SED. It is well known that a narrow relation exists between K -band and redshift as observed in Hubble diagrams (De Breuck et al. 2002; Willott et al. 2003; Jarvis et al. 2001; Eales & Rawlings 1993). In this work we construct a Hubble diagram of USS radio sources in the optical r band to $z \sim 0.8$. Despite any k-correction and possible extinction effects, our r band Hubble diagram (Figure 6) also clearly shows a tight correlation. We find that USS radio sources are as bright as central galaxies in the maxBCG cluster sample and are typically more than 4 magnitudes brighter than normal galaxies at $z \sim 0.3$. We note that this result is not entirely new, for example De Breuck et al. (2002) also find that at redshifts < 1 radio-loud galaxies define the luminous envelope using near infrared K -band magnitudes.

Regarding the possible dependence of radio luminosity on environment, we notice that the radio luminosity distribution of USS, radio sources in general, and radio sources in

clusters are remarkably similar (Figure 4), indicating that USS prefer higher density environments, independent of radio luminosity. These results are consistent with those by Hill & Lilly (fig. 8, 1991) who find no significant correlation in cluster richness $N_{0.5}$ and the rest-frame 2.0 GHz radio power for a sample of radio sources with $z < 0.5$. Similar results were obtained by Allington-Smith et al. (1993) who find no trend of richness with radio luminosity at 408 MHz for a sample of radio sources with $z < 0.5$.

We also analyze the richness and spectral index properties of clusters of galaxies associated with radio sources and find that 40% of USS sources identified in the SDSS spectroscopic catalogue are associated with cluster or groups of galaxies identified in the literature, such as in the maxBCG, Abell, or Zwicky catalogues. We analyze the local density of galaxies around the sample of USS sources without a known cluster association from the literature, using the Σ_5 and N1 estimators and find that these USS sources have similar galaxy densities to clusters selected from the maxBCG catalogue.

We also find that USS sources at low redshift are rare objects (99 from a total sample of 2885 radio sources detected in the SDSS spectroscopic catalogue). However a majority reside in regions of unusually high ambient density, such as those regions found in rich cluster of galaxies.

Our results complement those found by De Breuck et al. (2000). These authors define a sample of 669 USS sources selected from the WENSS, TEXAS, MRC, NVSS and PMN radio surveys. They conclude that the majority of relative nearby ($z < \sim 0.4$) USS objects are located in galaxy clusters. They find that at least 85% of the X-ray objects associates with USS sources are galaxy clusters or known groups from the literature.

At lower redshifts, we find that radio sources with $\alpha_{325}^{1400} < -0.65$, are preferentially located in galaxy cluster environments. This result contrast with Prestage & Peacock (fig. 7, 1988) where it is found no dependence of the spatial cross-correlation amplitude on spectral index. We note although that this statistical analysis concerns more the large-scale, rather than the local environment of our study.

We also find that clusters hosting radio sources with spectra steeper than the average have a higher galaxy richness and are populated by brighter galaxies in comparison to clusters associated to radio sources with $\alpha_{325}^{1400} > -0.65$. A natural explanation for these correlations is that radio emission in rich cluster of galaxies is pressure-confined in a high gas density environment. Radio lobes in galaxy cluster environment will expand adiabatically and lose energy via synchrotron and inverse Compton losses, resulting in a steeper radio spectra (Klamer et al. 2006).

9 ACKNOWLEDGMENTS

We are grateful to the anonymous referee for his/her careful reading of the manuscript and a number of comments, which improved the paper. This work was partially supported by the Consejo Nacional de Investigaciones Científicas y Técnicas (CONICET), the Secretaría de Ciencia y Técnica de la Universidad Nacional de Córdoba. The authors made use of the database CATS (Verkhodanov et al. 1997) of the Special Astrophysical Observatory and the NASA/IPAC extragalactic database (NED) which is operated by the Jet Propulsion Laboratory, Caltech, under contract with the National Aeronautics and Space Administration. This publication makes use of data products from the Sloan Digital Sky Survey (SDSS). Funding for the SDSS and SDSS-VI has been provided by the Alfred P. Sloan Foundation, the Participating Institutions, the National Science Foundation, the U.S. Department of Energy, the National Aeronautics and Space Administration, the Japanese Monbukagakusho, the Max Planck Society, and the Higher Education Funding Council for England. The SDSS Web Site is <http://www.sdss.org/>. The SDSS is managed by the Astrophysical Research Consortium for the Participating Institutions. The Participating Institutions are the American Museum of Natural History, Astrophysical Institute Potsdam, University of Basel, University of Cambridge, Case Western Reserve University, University of Chicago, Drexel University, Fermilab, the Institute for Advanced Study, the Japan Participation Group, Johns Hopkins University, the Joint Institute for Nuclear Astrophysics, the Kavli Institute for Particle Astrophysics and Cosmology, the Korean Scientist Group, the Chinese Academy of Sciences (LAMOST), Los Alamos National Laboratory, the Max-Planck-Institute for Astronomy (MPIA), the Max-Planck-Institute for Astrophysics (MPA), New Mexico State University, Ohio State University, University of Pittsburgh, University of Portsmouth, Princeton University, the United States Naval Observatory, and the University of Washington.

REFERENCES

- Allington-Smith, J. R., Ellis, R., Zirbel, E. L., & Oemler, A. J. 1993, *ApJ*, 404, 521
- Abell, G. O., Corwin, H. G., Jr., & Olowin, R. P. 1989, *ApJS*, 70, 1
- Baldwin, J. E., & Scott, P. F. 1973, *MNRAS*, 165, 259
- Best, P. N., von der Linden, A., Kauffmann, G., Heckman, T. M., & Kaiser, C. R. 2007, *MNRAS*, 379, 894
- Blanton, M. R., & Roweis, S. 2007, *AJ*, 133, 734
- Blundell, K. M., & Rawlings, S. 1999, *Nature*, 399, 330
- Blundell, K. M., Rawlings, S., & Willott, C. J. 1999, *AJ*, 117, 677
- Broderick, J. W., Bryant, J. J., Hunstead, R. W., Sadler, E. M., & Murphy, T. 2007, *MNRAS*, 381, 341
- Chambers, K. C., Miley, G. K., & van Breugel, W. J. M. 1990, *ApJ*, 363, 21
- Chambers, K. C., Miley, G. K., van Breugel, W. J. M., & Huang, J.-S. 1996, *ApJS*, 106, 215
- Cohen, A. S., Röttgering, H. J. A., Jarvis, M. J., Kassim, N. E., & Lazio, T. J. W. 2004, *ApJS*, 150, 417
- Cohen, A. S., Lane, W. M., Kassim, N. E., Lazio, T. J. W., Cotton, W. D., Perley, R. A., Condon, J. J., & Erickson, W. C. 2006, *Astronomische Nachrichten*, 327, 262
- Cowie, L. L., Barger, A. J., Hu, E. M., Capak, P., & Songaila, A. 2004, *AJ*, 127, 3137
- Cruz, M. J., et al. 2006, *MNRAS*, 373, 1531
- De Breuck, C., van Breugel, W., Röttgering, H. J. A., & Miley, G. 2000, *A&AS*, 143, 303
- De Breuck, C., van Breugel, W., Stanford, S. A., Röttgering, H., Miley, G., & Stern, D. 2002, *AJ*, 123, 637
- Eales, S. A., & Rawlings, S. 1993, *ApJ*, 411, 67
- Fukugita, M., Ichikawa, T., Gunn, J. E., Doi, M., Shimasaku, K., & Schneider, D. P. 1996, *AJ*, 111, 1748
- Geach, J. E., Simpson, C., Rawlings, S., Read, A. M., & Watson, M. 2007, *MNRAS*, 381, 1369
- Gopal-Krishna 1988, *A&A*, 192, 37
- Hansen, S. M., McKay, T. A., Wechsler, R. H., Annis, J., Sheldon, E. S., & Kimball, A. 2005, *ApJ*, 633, 122
- Hill, G. J., & Lilly, S. J. 1991, *ApJ*, 367, 1
- Intema, H. T., Venemans, B. P., Kurk, J. D., Ouchi, M., Kodama, T., Röttgering, H. J. A., Miley, G. K., & Overzier, R. A. 2006, *A&A*, 456, 433
- Jarvis, M. J., Rawlings, S., Eales, S., Blundell, K. M., Bunker, A. J., Croft, S., McLure, R. J., & Willott, C. J. 2001, *MNRAS*, 326, 1585
- Jarvis, M. J., Cruz, M. J., Cohen, A. S., Röttgering, H. J. A., & Kassim, N. E. 2004, *MNRAS*, 355, 20
- Kajisawa, M., Kodama, T., Tanaka, I., Yamada, T., & Bower, R. 2006, *MNRAS*, 371, 577
- Kimball, A. E., & Ivezić, 2008, *AJ*, 136, 684
- Klamer, I. J., Ekers, R. D., Bryant, J. J., Hunstead, R. W., Sadler, E. M., & De Breuck, C. 2006, *MNRAS*, 371, 852
- Koester, B. P., et al. 2007a, *ApJ*, 660, 239
- Koester, B. P., et al. 2007b, *ApJ*, 660, 221
- Krolik, J. H., & Chen, W. 1991, *AJ*, 102, 1659
- Kurk, J. D., Pentericci, L., Röttgering, H. J. A., & Miley, G. K. 2004a, *A&A*, 428, 793
- Kurk, J. D., Pentericci, L., Overzier, R. A., Röttgering, H. J. A., & Miley, G. K. 2004b, *A&A*, 428, 817
- Laing, R. A., & Peacock, J. A. 1980, *MNRAS*, 190, 903
- Le Fèvre, O., et al. 2005, *A&A*, 439, 845
- Lilly S.J., Longair M.S., 1984, *MNRAS*, 211, 833
- Lilly, S. J. 1988, *ApJ*, 333, 161
- Lopes, P. A. A., de Carvalho, R. R., Gal, R. R., Djorgovski, S. G., Odewahn, S. C., Mahabal, A. A., & Brunner, R. J. 2004, *AJ*, 128, 1017
- Miley, G. K., et al. 2004, *Nature*, 427, 47
- Miley, G. K., et al. 2006, *ApJ*, 650, L29
- O’Mill, A. L., Padilla, N., & Lambas, D. G. 2008, *MNRAS*, 389, 1763
- Overzier, R. A., et al. 2006, *ApJ*, 637, 58
- Oyaizu, H., Lima, M., Cunha, C. E., Lin, H., Frieman, J., & Sheldon, E. S. 2008, *ApJ*, 674, 768
- Prestage, R. M., & Peacock, J. A. 1988, *MNRAS*, 230, 131
- Roettgering, H. J. A., van Ojik, R., Miley, G. K., Chambers, K. C., van Breugel, W. J. M., & de Koff, S. 1997, *A&A*, 326, 505
- Slingo, A. 1974, *MNRAS*, 168, 307
- Venemans, B. P., et al. 2002, *ApJ*, 569, L11
- Venemans, B. P., et al. 2007, *A&A*, 461, 823
- Verkhodanov, O. V., Trushkin, S. A., & Chernenkov, V. N. 1997, *Baltic Astronomy*, 6, 275
- Villar-Martín, M., Sánchez, S. F., Humphrey, A., Dijkstra, M., di Serego Alighieri, S., De Breuck, C., & González Delgado, R. 2007, *MNRAS*, 378, 416
- West, M. J. 1994, *MNRAS*, 268, 79
- Willott, C. J., Rawlings, S., Jarvis, M. J., & Blundell, K. M. 2003, *MNRAS*, 339, 173
- Zwicky, F., & Kowal, C. T. 1968, "Catalogue of Galaxies and of Clusters of Galaxies", 1968, Volume VI Pasadena: California Institute of Technology, CGCG6,

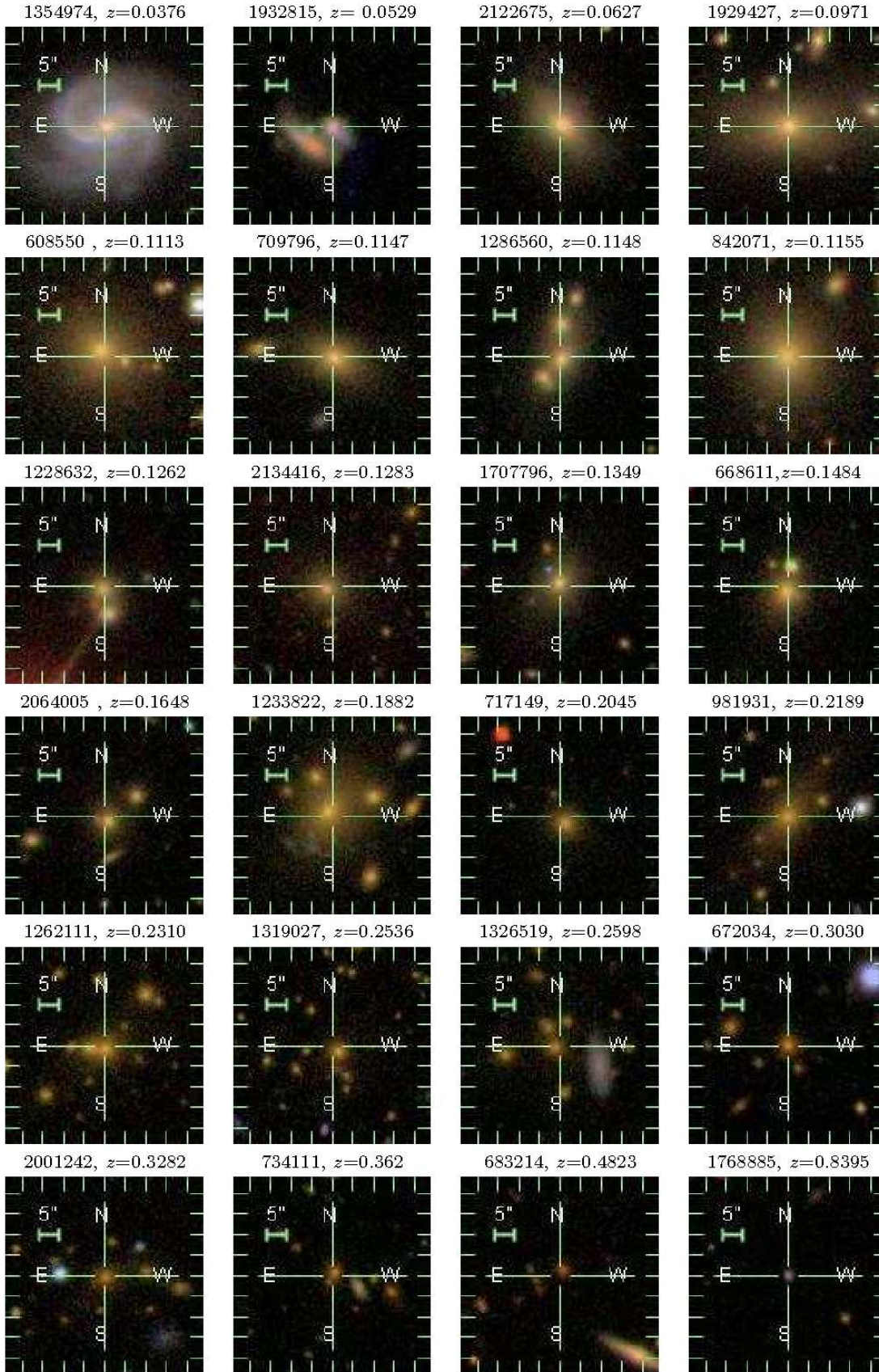


Figure 14. Cutout colour images of a subsample of galaxies associated with Ultra Steep radio sources in the SDSS catalogue. The open cross indicates the radio position taken from the FIRST survey. The ID and redshift (increasing from left to right) are indicated above each plot. Information for the complete sample is listed in Table 1.

Table 1. Sample of USS radio sources in the SDSS catalogue with spectroscopic redshifts.

ID	R.A. _{J2000} h m s	DEC _{J2000} ° ′ ″	z	α_{352}^{1400}	Log($L_{1.4}$) W Hz ⁻¹	M_r	ID from literature Designation
608550	07 25 57.08	+41 23 05.13	0.1113	-1.40	23.76	-22.18	MaxBCG J111.48808+41.38519
664059	07 51 31.86	+43 49 29.49	0.4249	-1.00	24.22	-22.63	...
668611	07 53 32.47	+38 57 52.71	0.1484	-1.04	23.37	-21.71	...
672034	07 54 57.66	+38 15 22.71	0.3030	-1.10	23.73	-20.00	...
683214	07 59 49.48	+35 32 33.82	0.4823	-1.04	25.19	-22.54	...
709796	08 10 54.66	+49 11 03.90	0.1147	-1.24	23.28	-22.27	MaxBCG J122.72750+49.18436
717149	08 13 50.80	+39 32 32.11	0.2045	-1.03	23.90	-21.79	MaxBCG J123.46125+39.54183
734111	08 20 32.39	+30 34 48.65	0.3628	-1.04	25.98	-21.97	...
735423	08 21 03.64	+52 44 35.82	0.4441	-1.38	25.08	-22.79	...
748224	08 26 00.38	+40 58 51.75	0.0576	-1.11	22.78	-22.79	SDSS-C4-DR3 3247
780016	08 38 23.27	+29 45 21.67	0.1068	-1.06	22.68	-22.00	SHK 182 GGroup
794634	08 43 59.18	+51 05 25.55	0.1264	-1.12	24.37	-22.63	...
801800	08 46 37.85	+51 27 16.56	0.1800	-1.27	23.88	-21.71	MaxBCG J131.65796+51.45436
814626	08 51 17.29	+37 04 29.00	0.2207	-1.00	24.11	-20.32	...
837935	08 59 57.32	+56 47 12.15	0.1833	-1.06	23.71	-22.11	...
838957	09 00 20.28	+52 29 39.73	0.0302	-1.02	22.01	-24.49	CGCG 264-047
842071	09 01 30.10	+55 39 16.42	0.1155	-1.80	23.81	-22.75	MaxBCG J135.37558+55.65463
846087	09 03 00.14	+35 27 04.82	0.3488	-1.01	25.53	-21.09	...
848084	09 03 44.85	+41 38 19.31	0.2189	-1.01	24.42	-21.42	MaxBCG J135.93682+41.63908
932725	09 34 42.25	+35 14 16.48	0.4618	-1.15	24.31	-22.62	...
940538	09 37 37.11	+37 05 35.37	0.4492	-1.01	25.24	-22.53	...
955678	09 43 09.29	+29 50 18.31	0.2969	-1.05	24.42	-18.71	...
981931	09 52 49.14	+51 53 04.99	0.2151	-1.77	24.08	-22.49	ZwCl 0949.6+5207
989139	09 55 29.87	+60 23 17.47	0.1989	-1.55	23.82	-22.03	MaxBCG J148.87452+60.38814
1002970	10 00 31.01	+44 08 42.94	0.1533	-1.44	23.16	-21.32	RBS 0819
1027752	10 09 28.28	+46 17 37.17	0.3858	-1.04	24.29	-19.86	...
1051000	10 17 58.13	+37 10 54.02	0.0442	-1.16	22.04	-22.34	CGCG 183-009
1075981	10 27 09.98	+39 08 06.04	0.3378	-1.02	24.93	-23.20	...
1080596	10 28 54.68	+48 09 38.20	0.4851	-1.45	24.99	-22.19	...
1109542	10 39 32.11	+46 12 05.54	0.1864	-1.21	24.85	-21.92	...
1128337	10 46 25.51	+59 37 37.59	0.2282	-1.07	23.56	-22.91	MaxBCG J161.60635+59.62690
1138526	10 50 10.03	+32 22 05.09	0.1150	-1.33	23.01	-21.94	NSCS J105005+322256 /CLtr
1160615	10 58 19.46	+41 03 40.76	0.1299	-1.07	23.41	-22.44	MaxBCG J164.58100+41.06140
1177112	11 04 33.11	+46 42 25.96	0.1410	-1.82	23.45	-21.08	...
1179743	11 05 30.73	+31 14 36.74	0.4381	-1.43	24.12	-21.34	...
1216462	11 18 45.25	+52 16 00.95	0.4309	-1.24	24.60	-22.18	...
1228632	11 23 22.90	+47 55 14.34	0.1262	-1.03	22.91	-21.08	...
1233822	11 25 16.31	+42 29 10.97	0.1882	-1.02	24.12	-23.00	ABELL 1253
1239404	11 27 18.46	+53 02 21.12	0.3236	-1.04	24.49	-23.56	...
1244341	11 29 01.60	+32 45 50.65	0.5759	-1.10	25.02	-22.24	...
1250737	11 31 20.94	+33 34 46.95	0.2219	-1.61	23.72	-22.26	MaxBCG J172.83707+33.57975
1260844	11 34 57.39	+53 46 24.20	0.1695	-1.05	23.24	-21.52	...
1262111	11 35 26.68	+31 53 33.14	0.2310	-1.05	24.71	-22.67	MACS J1135.4+3153
1268493	11 37 50.23	+46 36 33.65	0.3151	-1.03	24.72	-23.08	...
1286560	11 44 27.21	+37 08 32.42	0.1148	-1.56	23.55	-21.11	...
1294316	11 47 12.35	+38 19 26.32	0.5977	-1.01	25.34	-22.11	...
1304138	11 50 49.21	+62 19 49.04	0.3453	-1.69	24.37	-23.04	...
1307368	11 51 58.63	+31 40 32.05	0.5079	-1.04	25.69	-23.39	...
1307436	11 52 00.09	+33 13 42.49	0.3573	-1.48	23.97	-23.15	...

Table 1.

ID	R.A. ^{radio} _{h m s} J_{2000}	DEC ^{radio} _{° ′ ″} J_{2000}	z	α_{352}^{1400}	Log($L_{1.4}$) W Hz ⁻¹	M_r	ID from literature Designation
1309157	11 52 36.33	+37 32 43.86	0.2294	-1.19	24.22	-20.23	MaxBCG J178.15191+37.54548
1319027	11 56 05.51	+34 33 05.33	0.2536	-1.10	25.05	-21.83	[EAD2007] 200 Arcs
1326519	11 58 48.07	+57 17 19.11	0.2598	-1.04	25.12	-24.49	...
1348701	12 06 47.88	+51 57 10.95	0.3446	-1.28	24.66	-21.51	...
1351855	12 08 00.78	+43 39 19.12	0.2657	-1.00	24.77	-22.57	MaxBCG J182.00318+43.65537
1353531	12 08 37.16	+61 21 06.52	0.2748	-1.48	23.96	-22.17	...
1354974	12 09 08.84	+44 00 11.30	0.0376	-1.12	22.12	-22.98	NGC4135, (G. group)
1362044	12 11 46.22	+32 38 38.16	0.6115	-1.07	24.94	-22.25	...
1406400	12 28 02.17	+34 40 40.12	0.2775	-1.40	23.81	-22.53	MaxBCG J187.00902+34.67753
1439302	12 40 04.88	+37 44 15.46	0.1879	-1.15	23.75	-21.53	NSC J124001+374544
1468909	12 51 07.51	+56 25 44.98	0.2008	-1.22	23.42	-21.73	...
1505383	13 04 31.36	+51 43 42.64	0.2757	-1.56	24.43	-22.28	MaxBCG J196.15441+51.71551
1510127	13 06 12.17	+51 44 06.94	0.2773	-1.16	24.55	-22.54	MaxBCG J196.55069+51.73530
1532575	13 14 18.32	+41 24 30.18	0.1987	-1.05	23.25	-20.90	MaxBCG J198.57609+41.40825
1547051	13 19 38.92	+61 39 11.68	0.1333	-1.21	23.49	-22.47	...
1559285	13 24 12.38	+31 17 24.33	0.4268	-1.19	24.63	-22.47	...
1604023	13 40 32.89	+40 17 38.79	0.1719	-1.17	23.32	-22.35	RX J1340.5+4017 GGroup
1607910	13 41 59.68	+42 21 32.32	0.4261	-1.22	24.07	-22.75	...
1627288	13 49 03.74	+30 52 27.51	0.0814	-1.13	22.53	-19.43	...
1628350	13 49 27.88	+46 20 15.29	0.4212	-1.14	24.17	-14.98	...
1673236	14 06 03.34	+52 09 51.98	0.4823	-1.01	24.75	-23.38	...
1707796	14 18 37.62	+37 46 22.63	0.1349	-1.34	23.37	-21.87	ABELL 1896
1714152	14 20 56.84	+53 13 07.25	0.7430	-1.05	25.29	-23.57	...
1714768	14 21 10.18	+42 09 12.97	0.3529	-1.12	24.03	-20.99	NSCS J142115+420743
1735168	14 28 41.23	+43 41 34.03	0.2136	-1.04	23.70	-22.42	NSCS J142842+434009
1735918	14 28 57.67	+54 36 27.65	0.3819	-1.50	24.39	-21.60	...
1744373	14 32 04.05	+46 37 43.79	0.0927	-1.03	22.65	-19.72	NSC J143143+463738
1755382	14 36 02.53	+33 07 53.79	0.0939	-1.02	22.80	-20.51	...
1756038	14 36 19.44	+48 32 10.68	0.1912	-1.07	24.03	-21.62	...
1759889	14 37 42.41	+39 27 45.12	0.2455	-1.36	24.35	-21.94	MaxBCG J219.42655+39.46313
1768885	14 40 57.03	+46 36 46.91	0.8395	-1.12	25.35	-19.00	...
1775379	14 43 17.07	+46 43 48.40	0.2424	-1.34	23.68	-21.83	...
1793973	14 50 03.51	+31 30 15.02	0.2746	-1.10	24.25	-21.95	MaxBCG J222.55394+31.49750
1795282	14 50 31.54	+32 53 03.73	0.1775	-1.38	23.45	-21.67	...
1830754	15 03 23.78	+46 06 16.28	0.4269	-1.06	24.19	-22.74	...
1836180	15 05 23.43	+47 06 25.59	0.2615	-1.63	23.90	-22.52	ABELL 2024
1837171	15 05 46.23	+54 54 01.56	0.2824	-1.24	24.49	-22.69	...
1838173	15 06 08.41	+60 02 16.86	0.5196	-1.03	24.72	-24.11	...
1862173	15 15 05.54	+43 09 01.38	0.0177	-1.14	21.11	-23.69	CGCG 221-045
1929427	15 39 50.77	+30 43 03.90	0.0971	-1.18	23.10	-22.36	MaxBCG J234.96158+30.71777
1932815	15 41 05.46	+32 04 50.85	0.0529	-1.06	22.51	-20.79	...
1934628	15 41 46.53	+45 56 14.29	0.2024	-1.08	24.31	-21.37	...
1958800	15 50 51.44	+42 02 30.47	0.0334	-1.09	21.91	-20.61	...
1963482	15 52 41.11	+37 24 34.16	0.3710	-1.92	24.23	-23.69	...
1967858	15 54 23.54	+48 41 07.36	0.2271	-1.04	23.93	-22.32	MaxBCG J238.59817+48.68496
2001242	16 07 25.43	+47 50 24.15	0.3282	-1.02	24.76	-22.54	ABELL 2157
2064005	16 33 10.92	+36 07 35.15	0.1648	-1.02	23.93	-21.42	MaxBCG J248.29532+36.12611
2088195	16 43 26.82	+39 30 39.92	0.4119	-1.05	24.72	-22.15	...
2122675	16 59 01.01	+32 29 38.93	0.0627	-1.26	23.82	-21.61	ABELL 2241
2134416	17 04 26.40	+39 10 12.25	0.1283	-1.01	23.23	-21.34	NSC J170432+390956